Second-Time Fault-Tolerant Topology and Control Strategy for the Open-Winding PMSM System Based on Shared Bridge Arm

Xiaoguang Zhang, *Member, IEEE*, and Chi Xu

***Abstract*—To further improve the fault-tolerant operation capacity of the open-winding permanent magnet synchronize motor system after second-time fault occurring, a novel fault-tolerant topology and a fault-tolerant control strategy for single phase open-circuit is proposed in this article. The fault-tolerant topology proposed in this article can operate stably in case of second-time fault that occurs after one-phase open-circuit fault by the way of sharing a bridge arm. Thus, the fault-tolerant ability of the driving system is further improved. In the terms of control strategy, the amplitude and the phase of the remaining two-phase current are redesigned to keep the system operating steadily according to the conventional expression of motor torque. Moreover, considering that the electromagnetic torque of the system will contain the third harmonic component when the three-phase current is unbalanced, the torque fluctuation will affect the stability of the system. A torque optimization strategy for suppressing the third harmonic component of the torque by injecting corresponding harmonics into the current is proposed. Finally, the experimental results validate the effectiveness of the proposed topology and strategy.**

***Index Terms*—Fault tolerance, open winding, permanent magnet synchronize motor (PMSM), third harmonic component, topology, torque.**

I. Introduction

THE permanent magnet synchronize motor (PMSM) has been widely studied and applied in industrial and electric vehicle field due to its high efficiency, large torque-current ratio, high power-weight ratio, high power factor, and good control performance [1]–[3]. However, with the increasing demand of driving system performance, the reliability has become the focus of attention. The conventional PMSM has insufficient fault tolerance due to its inherent topology limitation, and its application in high power field is restrained by the capacity of switching devices [4], [5].

In order to overcome the deficiencies of the conventional PMSM mentioned above, the open-winding permanent magnet synchronize motor (OW-PMSM) is formed by opening the neutral point of the traditional PMSM windings and supplying power from both ends of the winding with two inverters. The OW-PMSM retains all the advantages of traditional PMSM without changing the overall structure of the motor, while decoupling the three-phase windings greatly improves its fault tolerant capability [6]–[9]. Furthermore, the system capacity of the OW-PMSM topology can be doubled and the output voltage vector is the same as that of three-level inverters, but compared with the traditional three-level inverters, the cost can be saved because no clamping diodes are needed [10]–[12]. Therefore, the OW-PMSM system is very suitable for high power and strong reliability occasions.

The ability of driving system to withstand faults is critical for stable operation. In order to improve the reliability of the OW-PMSM driving system, some methods have been proposed. In [13], a simplified pulsewidth modulation (PWM) for fault-tolerant control of OW-PMSM fed by hybrid inverter is proposed. In [14], the fault-tolerant control strategy of an open-end winding system driven by single power supply under six switching devices open-circuit fault is proposed where the direct torque control (DTC) algorithm is adopted for the postfault operation. In addition, according to the distribution of vectors in fault state, a modulation scheme using two orthogonal voltage vectors to synthesize target voltage is proposed in [15] to realize the fault-tolerant operation of inverter fault. In [16], an open-winding five-phase driving system with short-circuit fault on switching devices is considered, the driving system can keep the torque unchanged under fault condition by reconstructing the structure of faulty inverter simply and utilizing the inherently switching states. In [17], a hybrid modulation fault-tolerant control of an open-end winding linear vernier permanent-magnet (OEW-LVPM) motor is presented. When the open-circuit fault of power switching occurs, this OEW-LVPM system is able to achieve steady operation. The work in [18] presents the fault-tolerant strategy of the open-winding motor system when different fault occurs. Thus, the continuous operation can be achieved under the control of this control strategy by reconstructing the neutral point of motor.

Manuscript received September 13, 2019; revised December 19, 2019, February 19, 2020, and April 10, 2020; accepted April 20, 2020. Date of publication April 26, 2020; date of current version July 20, 2020. This work was supported in part by the National Natural Science Foundation of China under Grant 51877002, in part by the Outstanding Young Scholars Fund of North China University of Technology, in part by the Young TopNotch Talents Program of Beijing Excellent Talents Funding (2017000026833ZK12), in part by the Fundamental Research Funds for Beijing Universities under Project 110052971921/025, in part by the Young TopNotch Talents Program for Municipal Universities of Beijing (CIT&TCD201904011), and in part by the 2019 Beijing Nova Program (Z191100001119036). Recommended for publication by Associate Editor A. J. M. Cardoso. (*Corresponding author: Xiaoguang Zhang*.)

The authors are with the North China University of Technology, Beijing 100144, China (e-mail: zhangxg123456789@163.com; 1107750848@qq.com).

Color versions of one or more of the figures in this article are available online at https://ieeexplore.ieee.org.

Digital Object Identifier 10.1109/TPEL.2020.2990303

In addition, there are some research results on the fault-tolerant operation of dual inverter topology. Freire has very rich research results and put forward a variety of fault-tolerant topologies, among which the topology in [19] and [20] stands out due to the lower cost and better performance. In [19] and [20], fault-tolerant operation is realized by replacing fault bridge arm by connecting dc bus midpoint with TRIAC, but the difference is that the topology in [19] use three TRIACs and cannot deal with the simultaneous fault of the inverter on both side at the same time, while the topology in [20] can deal with this problem by using six TRIACs. In [21]–[23], according to the idea of five-leg operation of back-to back inverter, fault-tolerant operation is realized by turning on the fault phase TRIAC to make the front and rear stages share the same bridge leg after the fault occurs. It can be found that the idea of bridge arm sharing is very interesting, although this kind of topology increases the cost of the system and sacrifices the capacity of original system after fault occurs, it provides a simple way to realize the fault-tolerant operation of dual inverter system.

Although the existing work can achieve effective fault-tolerance control of the open-winding motor system, the second-time fault-tolerant problem is not considered, and no second-time fault-tolerant topology and control strategy are reported in the OW-PMSM system. In order to further improve the fault-tolerant performance of the OW-PMSM driving system, based on the idea of bridge arm sharing, the control of driving system after the second-time open-circuit fault of the remaining inverter power devices during one-phase open-circuit fault operation is researched in this article. The remainder of this article is organized as follows. In Section II, a novel fault-tolerant topology is proposed by analyzing the voltage vector generated by the conventional fault-tolerant topology. In Section III, the mathematical model of OW-PMSM is introduced and based on it, the fault-tolerant control method and the suppression strategy of torque ripple under second-time open-circuit fault are proposed. Moreover, to study the capacity change of system after fault occurs, the speed and torque output ability are analyzed in Section IV. Then, experimental results are carried out to validate the effectiveness of the proposed fault-tolerant topology and control strategy in Section V. Finally, Section VI concludes this article.

II. Proposed Fault-Tolerant Topology and Its Voltage Vectors

In this section, the one-time fault-tolerant topology of the OW-PMSM system is introduced first. Then, in order to further improve the fault-tolerant operation ability of the OW-PMSM system after second-time open-circuit fault, a novel fault-tolerant topology for single phase open-circuit is proposed.

A. One-Time Fault-Tolerant Topology of the OW-PMSM System With Single Phase Open-Circuit

The one-time fault-tolerant topology of OW-PMSM system with single phase open-circuit is shown in Fig. 1. The OW-PMSM is driven by two-phase full-leg inverter, which includes four bridge arms and eight switching devices. In this topology, there are 16 combinations of switching states, which can

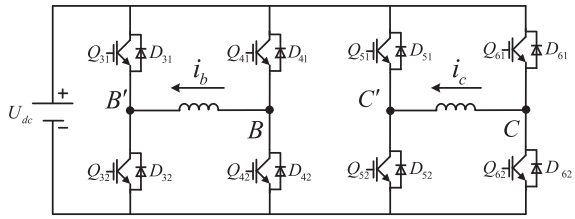

Fig. 1. OW-PMSM system one-time fault-tolerant topology.

TABLE I
Switching States and Voltages of Conventional Topology

Vectors	u_0	u_1	u_2	u_3	u_4	u_5	u_6	u_7	u_8
$S^{B'}S^{B}S^{C'}S^{C}$	0000, 0011, 1100, 1111	0101	0001, 1101	1000, 1011	1010	0010, 1110	0100, 0111	1001	0110
u_b	0	U_{dc}	0	$-U_{dc}$	$-U_{dc}$	0	U_{dc}	$-U_{dc}$	U_{dc}
u_c	0	U_{dc}	U_{dc}	0	$-U_{dc}$	$-U_{dc}$	0	U_{dc}	$-U_{dc}$

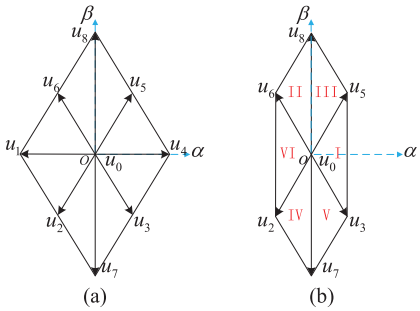

Fig. 2. Voltage vector distribution. (a) Voltage vectors generated by one-time topology. (b) Voltage vector generated by the proposed second-time topology.

generate 9 kinds of effective voltage vectors. In this article, the current that flows from winding terminal $B(C)$ to winding terminal $B^{'}(C^{'})$ is considered as the positive phase current, then the relationship between phase voltages, voltage vectors and switching states shown in Table I can be obtained.

The distribution of voltage vectors generated by this fault-tolerant topology is shown in Fig. 2(a), including one zero vector and eight nonzero vectors. Among these eight nonzero voltage vectors, the amplitudes of $u_1 - u_6$ are $2U_{\rm dc}/3$ and the other two voltage vectors have an amplitude of $2\sqrt{3}U_{\rm dc}/3$. These nine voltage vectors can be used to drive the OW-PMSM system to achieve fault-tolerant operation.

By analyzing the voltage vectors of this topology and its switching states, it can be found that the voltage vectors u_1, u_4, u_7, and u_8 are formed by single switching states, and the voltage vectors u_0, u_2, u_3, u_5, and u_6 are formed by different switching states. For example, the switching state (0001) and the switching state (1101) both can generate voltage vector u_2; however, it should be noted that, when the switching state (0001) is applied to form vector u_2, the B and C$^{'}$ arms have the same switching state, i.e., $S^B = S^{C'} = 0$. Similarly, the switching states of remaining voltage vector u_0, u_3, u_5, and u_6 also have the same phenomenon. In addition, the voltage vector u_7 formed by single switching states (1001) has the same switching states "0" of the B and C$^{'}$ arms; the voltage vector u_8 formed by the switching

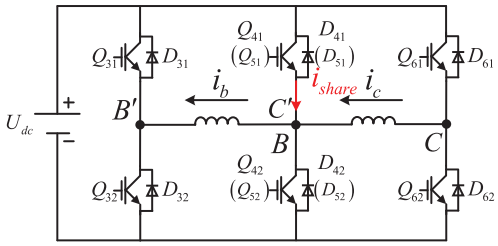

Fig. 3. Proposed second-time fault-tolerant topology of the OW-PMSM system with B and C' share a bridge arm.

states (0110) has the same switching states "1" of the B and C' arms.

Above analysis results indicate that the most voltage vectors in this topology can be obtained when the *B*-arm and the *C*'-arm are merged. This means that, when the open-circuit fault of the power switches in the *B*-arm or the *C*'-arm occur after A-phase open-circuit, the winding terminal *B* and *C*' can share a bridge arm to continue to ensure system operation, which increases the fault-tolerant ability of second-time fault.

B. Proposed Fault-Tolerant Topology of the OW-PMSM System With Single Phase Open-Circuit

The proposed second-time fault-tolerance topology of OW-PMSM system with single phase open-circuit fed by three-leg inverter is shown in Fig. 3. Compared with the one-time fault-tolerant topology, winding terminal *B* and *C*' share a bridge arm.

This novel topology includes three bridge arms (six switching devices), thus eight different working states can be obtained, as shown in Fig. 4. Fig. 4(a) and (b) describes the current flow path when the switching states are (000) and (111), respectively. Under these switching states, the winding terminal *B*, *B*', *C*, and *C*' are connected to the same point, thus the phase voltages of phase *B* and *C* are both 0. This means that the zero voltage vector u_0 can be formed. When the switching state is (001), the winding terminal *C* is connected to the positive pole of the dc bus, while the remaining winding terminals are connected to the negative pole of the dc bus, as shown in Fig. 4(c). In this case, the phase voltages of phase *B* and *C* are 0 and $U_{\rm dc}$, respectively, which can form the voltage vector u_2. Similarly, Fig. 4(d) describes the current flow path when the switching state is (100). The winding terminal *B*' is connected to the positive pole of the dc bus while other winding terminals are connected to the negative pole of the dc bus. Obviously, the phase voltages of phase *B* and *C* are $-U_{\rm dc}$ and 0, respectively; thus, the voltage vector as u_3 is generated. Using the similar way to analyze other switching states, the current flow path displayed in Fig. 4(e)–(h) can also be obtained. Then, according to the above analysis, the relationship during the phase voltages, the voltage vectors and the switching states of the proposed topology can be obtained, as shown in Table II.

From Table II, the voltage vector distribution of the proposed fault-tolerant topology can be gained, as shown in Fig. 2(b). Compared with the voltage vectors generated by the one-time topology, the proposed topology can generate seven kinds of voltage vectors, which are the same as the one-time topology

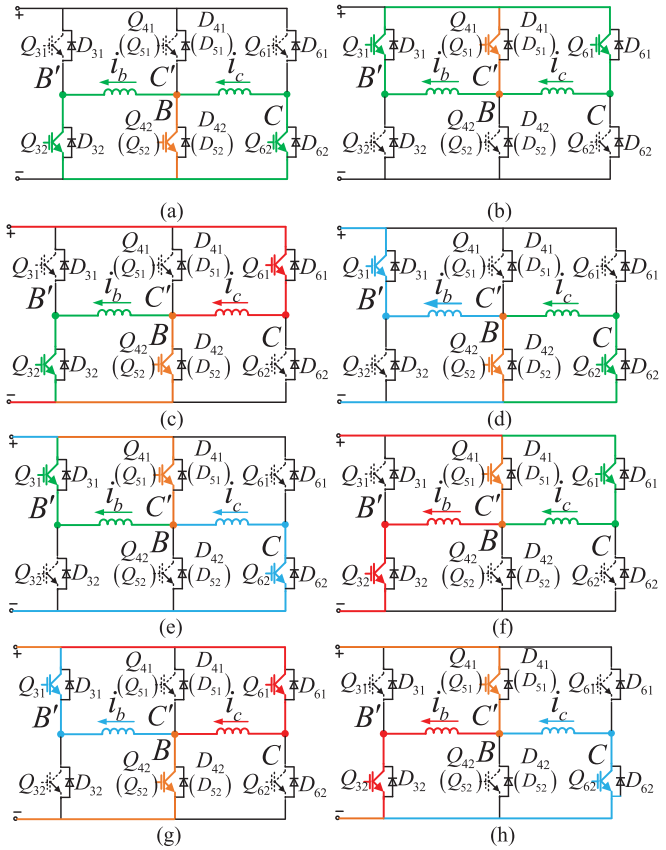

Fig. 4. Current flow path in proposed topology. (a) Switching state:000. (b) Switching state:111. (c) Switching state:001, (d) Switching state:100. (e) Switching state:110. (f) Switching state:011, (g) Switching state:101. (h) Switching state:010.

TABLE II
SWITCHING STATES AND VOLTAGES OF PROPOSED TOPOLOGY

Vectors	u_0	u_2	u_3	u_5	u_6	u_7	u_8
$S^{B'}S^{B}(S^{C'})S^{C}$	000, 111	001	100	110	011	101	010
u_b	0	0	$-U_{dc}$	0	U_{dc}	$-U_{dc}$	U_{dc}
u_c	0	U_{dc}	0	$-U_{dc}$	0	U_{dc}	$-U_{dc}$

except u_1 and u_4. Although the proposed topology generates less voltage vectors compared with the one-time topology due to the decrease of bridge arm, the smooth operation of the OW-PMSM system can be ensured by the proposed two-phase fault-tolerant control strategy in Section III.

Similarly, in all voltage vectors except u_1 and u_4, *B*' and *C* arms have the same switching state. This means that, when the open-circuit fault of the power switches in *B*'-arm or C-arm occurs after A-phase open-circuit, the winding terminal *B*' and C can share a bridge arm to continue to ensure system operation too. The reconfigured second-time fault-tolerant topology is shown in Fig. 5, and its voltage vectors are the same as in Fig. 2(b).

Obviously, redundant power devices are needed to realize the reconfiguration from one-time topology to second-time topology when the second-time fault occurs. In addition, for the one-time fault, it may occur in phase A, B, and C. Considering

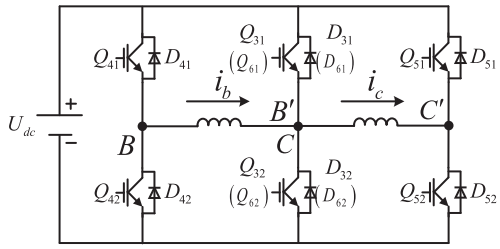

Fig. 5. Proposed second-time fault-tolerant topology of the OW-PMSM system with B' and C share a bridge arm.

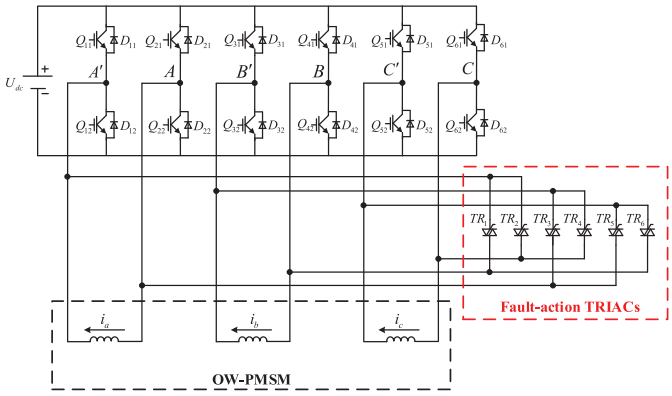

Fig. 6. Proposed fault-tolerant topology of the OW-PMSM system.

the possibility of all fault combinations, the topology as shown in Fig. 6 is proposed, which can realize the switching of the OW-PMSM system from healthy mode to one-time topology and then to second-time topology.

C. Proposed Fault-Tolerant Switching Topology of the OW-PMSM System

The OW-PMSM fault-tolerant topology that can realize one-time fault and second-time fault operation is shown in Fig. 6. Next, the switching method will be introduced in the following section.

1) One-Time Open-Circuit Fault: When the one-time fault occurs, the simplest and the lowest cost method is to discard the fault phase and use the remaining healthy winding to make the driving system run continuously by changing the control strategy. Taking A-phase open-circuit fault as an example, when the fault occurs, the one-time fault-tolerant topology of OW-PMSM system shown in Fig. 1 can be obtained by discarding the A-phase winding (without fault-action TRIACs behavior). The method of discarding phase can be divided into two categories: 1) for winding open-circuit, lock the gate signals of all A-phase switching devices; and 2) for the open-circuit fault of switching devices, lock the gate signal of Q_{12} and continually send the gate signals of Q_{11}, Q_{21}, and Q_{22} with a duty cycle of 0.5 [24]. And, the method of discarding phase B and C is similar.

2) Second-Time Open-Circuit Fault: When the OW-PMSM system is in fault-tolerant operation under the condition of single phase open-circuit, if the remaining healthy switching devices have open-circuit fault again, a new fault-tolerant topology can be constructed to realize the second-time fault-tolerant operation by the behavior of fault-action TRIACs. Taking the one-time fault tolerance of A-phase open-circuit as an example, if the B and C' bridge arms are in open-circuit fault of switching device (single device open-circuit fault, two devices in the same leg open circuit or two devices in different phase leg diagonal open circuit), as long as TR_6 is turned ON, the second-time fault-tolerant topology shown in Fig. 3 can be obtained; similarly, if the B' and C bridge arms are in open-circuit fault of switching devices, the second-time fault-tolerant topology as shown in Fig. 5 can also be gained by turning ON TR_4.

In addition, when one-time fault occurs in phase B (or in phase C), two kinds of second-time fault-tolerant topologies can be constructed by controlling TR_5 and TR_2 (or TR_3 and TR_1). In general, six kinds of second-time fault-tolerant topologies can be formed by controlling the fault-action TRIACs according to different fault combinations.

III. Proposed Fault-Tolerant Control Strategy

In the previous section, a novel topology is proposed and its voltage vectors are analyzed. In order to cooperate with this topology to control the OW-PMSM system with a good control performance, a fault-tolerant control strategy is proposed in this section. Since the OW-PMSM is driven by two-phase winding after one-phase fault occurs, torque control performance deteriorates. Therefore, a torque optimization method is proposed to suppress the fluctuation of the system's torque, which further improves the system control performance under the fault condition.

A. Mathematical Model of the OW-PMSM System

The voltage equation of the OW-PMSM system in the *abc*-coordinate can be written as follows:

$$\begin{bmatrix} u_a \\ u_b \\ u_c \end{bmatrix} = \begin{bmatrix} R00 \\ 0R0 \\ 00R \end{bmatrix} \begin{bmatrix} i_a \\ i_b \\ i_c \end{bmatrix} + \begin{bmatrix} LMM \\ MLM \\ MML \end{bmatrix} \frac{d}{dt} \begin{bmatrix} i_a \\ i_b \\ i_c \end{bmatrix} + \begin{bmatrix} e_a \\ e_b \\ e_c \end{bmatrix} \tag{1}$$

where *R*, *L*, and *M* are stator resistance, self-inductor and mutual inductor, respectively. u_k, i_k, and e_k ($k = a,b,c$) represent three-phase voltages, currents, and back electromotive force (EMFs), respectively. The back EMFs can be expressed as follows:

$$\begin{cases} e_a = -P\omega_m\psi_f \sin(\theta) - 3P\omega_m\psi_{f3}\sin(3\theta) \\ e_b = -P\omega_m\psi_f \sin(\theta - 2\pi/3) - 3P\omega_m\psi_{f3}\sin(3\theta) \\ e_c = -P\omega_m\psi_f \sin(\theta + 2\pi/3) - 3P\omega_m\psi_{f3}\sin(3\theta) \end{cases} \tag{2}$$

where *P*, ω_m, and ψ_f are the number of pole pairs, mechanical angular speed, and magnet flux linkage, respectively; θ is the electrical angle, and ψ_{f3} is the third harmonic component of the permanent magnetic flux linkage.

The electromagnetic torque of the OW-MPSM system in the *abc*-coordinate is expressed as follows:

$$T_e = \frac{e_a i_a + e_b i_b + e_c i_c}{\omega_m}. \tag{3}$$

In normal operating, three-phase balanced current shown in (4) is needed to ensure the stability of electromagnetic torque of the OW-MPSM system

$$\begin{cases} i_a = -I_m \sin(\theta) \\ i_b = -I_m \sin(\theta - 2\pi/3) \\ i_c = -I_m \sin(\theta + 2\pi/3) \end{cases} \tag{4}$$

where I_m is the amplitude of the three-phase current. Then, the torque can be expressed as follows:

$$T_{\text{ehealthy}} = \frac{3}{2} P \psi_f I_m. \tag{5}$$

Obviously, under the normal operation of the OW-PMSM system, only when the three-phase currents are in the same phase with the respective back EMF, can the motor obtain stable torque, and only in this way can the OW-PMSM system operate stably and reliably. However, under the fault condition (such as A-phase open-circuit), if the current of B-phase and C-phase is kept in phase with their own back EMF, the stable electromagnetic torque cannot be obtained. Therefore, in order to keep the system running stably in the fault-tolerant state, current control strategy need to be redesigned.

B. Redesigned Amplitude and Phase of Current

As analyzed above, in order to maintain the stability of the electromagnetic torque, the amplitude and phase of the current need to be redesigned. Assuming that A-phase winding open-circuit fault occurs and the phase difference of B-phase current and C-phase current is α and β, the three-phase current can be expressed as follows:

$$\begin{cases} i_a = 0 \\ i_b = -I_m \sin(\theta - \alpha) \\ i_c = -I'_m \sin(\theta - \beta) \end{cases} \tag{6}$$

where I_m and I'_m are the amplitude of i_b and i_c, respectively.

Combining (2), (3), and (6), the torque of the OW-PMSM system can be expressed as follows:

$$\begin{aligned} T_{\text{efault}} = {} & I_m P \psi_f \sin(\theta - 2\pi/3) \sin(\theta - \alpha) \\ & + I'_m P \psi_f \sin(\theta + 2\pi/3) \sin(\theta - \beta) \\ & + 3 I_m P \psi_{f3} \sin(\theta - \alpha) \sin(3\theta) \\ & + 3 I'_m P \psi_{f3} \sin(\theta - \beta) \sin(3\theta). \end{aligned} \tag{7}$$

Further simplification can obtain the following equation:

$$\begin{aligned} T_{\text{efault}} = {} & \frac{I_m P \psi_f}{2} [\cos(\alpha - 2\pi/3) - \cos(2\theta - \alpha - 2\pi/3)] \\ & + \frac{I'_m P \psi_f}{2} [\cos(\beta + 2\pi/3) - \cos(2\theta - \beta + 2\pi/3)] \\ & + 3 I_m P \psi_{f3} \sin(\theta - \alpha) \sin(3\theta) \\ & + 3 I'_m P \psi_{f3} \sin(\theta - \beta) \sin(3\theta). \end{aligned} \tag{8}$$

According to (8), it can be found that the electromagnetic torque under A-phase open-circuit will fluctuate due to the existence of variable θ in the expression. In addition, it is obvious that the torque is mainly generated by the first two items in (8), and the proportion of the last two items is small in the electromagnetic torque, since the third harmonic component of the permanent magnetic flux linkage ψ_{f3} is far smaller than the permanent magnetic flux linkage ψ_f. Therefore, in order to suppress the pulsating torque, the following condition must be satisfied to ensure the first two items can generate stable torque:

$$\begin{cases} I'_m = -I_m \\ \beta = \alpha + 4\pi/3 \end{cases}. \tag{9}$$

Then, substituting (9) into (8) one can obtain the following:

$$\begin{aligned} T_{\text{efault}} = {} & \frac{I_m P \psi_f}{2} [\cos(\alpha - 2\pi/3) - \cos(\beta + 2\pi/3)] \\ & + 3 I_m P \psi_{f3} \sin 3\theta [\sin(\theta - \alpha) - \sin(\theta - \beta)]. \end{aligned} \tag{10}$$

From (10), it is obvious that the maximal torque can be obtained under the fault condition when the angle α and β are selected as follows:

$$\begin{cases} \alpha = 5\pi/6 \\ \beta = \pi/6 \end{cases}. \tag{11}$$

Therefore, in order to ensure the motor can obtain stable and maximize torque, the remaining two-phase current needs to be designed according to the following rules:

$$\begin{cases} i_b = -I_m \sin(\theta - 5\pi/6) \\ i_c = -I_m \sin(\theta + 5\pi/6). \end{cases} \tag{12}$$

Similarly, the remaining healthy phase currents need to meet (13) and (14) respectively when the open-circuit fault occurs in B-phase or C-phase

$$\begin{cases} i_a = -I_m \sin(\theta + \pi/6) \\ i_c = -I_m \sin(\theta + \pi/2) \end{cases} \tag{13}$$

$$\begin{cases} i_a = -I_m \sin(\theta - \pi/6) \\ i_b = -I_m \sin(\theta - \pi/2). \end{cases} \tag{14}$$

C. Torque Optimization

According to the above analysis, it can be found that, when the angle α and β are selected according to (11), the maximal torque as shown in (15) can be obtained. The torque is mainly generated by the first item of (15), which is $1/\sqrt{3}$ times the normal torque (5), so it can be concluded that 42.26% of the output capacity of the torque is sacrificed when the system runs under second-time fault condition. Moreover, it is obvious that the second item in (15) is the harmonic component of the torque. Although torque harmonic amplitude $3\sqrt{3} I_m P \psi_{f3}$ is rather small compared with the main torque item $\sqrt{3} I_m P \psi_f / 2$, the torque instability will affect the control performance of the whole control system. Therefore, it is necessary to optimize the torque

$$T_{\text{efault}} = \frac{\sqrt{3} I_m P \psi_f}{2} - 3\sqrt{3} I_m P \psi_{f3} \sin\theta \sin 3\theta. \tag{15}$$

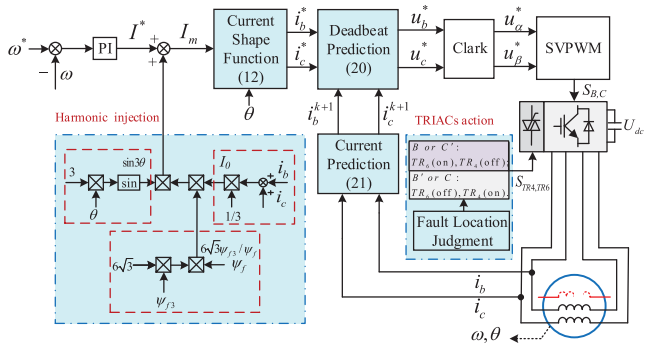

Fig. 7. Control diagram of the proposed control system.

According to (12), the zero sequence current of the one-phase open-circuit OW-PMSM system can be gained as follows:

$$I_0 = \frac{1}{3}\left(i_b + i_c\right) = \frac{\sqrt{3}}{3} I_m \sin(\theta). \tag{16}$$

Then, the torque expression (15) can be rewritten as follows:

$$T_{\text{efault}} = \frac{\sqrt{3} P \psi_f I_m}{2} - 9 P I_0 \psi_{f3} \sin 3\theta. \tag{17}$$

It can be seen from (17) that triple frequency torque component will cause the torque fluctuation and affect the system control performance, since the zero-sequence current is not zero. Therefore, in order to eliminate the torque fluctuation, a torque compensation strategy is presented. In this method, a harmonic torque $\frac{6\sqrt{3} I_0 \psi_{f3} \sin 3\theta}{\psi_f}$ is injected into the current amplitude I_m according to (17), then, compensated torque can be expressed as follows:

$$T_{\text{efault}} = \frac{\sqrt{3} P \psi_f}{2}\left(I_m + \frac{6\sqrt{3} I_0 \psi_{f3} \sin 3\theta}{\psi_f}\right)$$

$$- 9 P I_0 \psi_{f3} \sin 3\theta = \frac{\sqrt{3} P \psi_f}{2} I_m. \tag{18}$$

Therefore, the triple frequency torque $9 P I_0 \psi_{f3} \sin 3\theta$ of system torque can be eliminated by injecting harmonic into the current amplitude. The whole control diagram of the proposed fault-tolerant control method is shown in Fig. 7.

D. Deadbeat Current Control Under One Phase Fault Condition

1) Reference Voltage Prediction: Taking A-phase open-circuit as an example, after obtaining the current amplitude I_m with compensated torque, the B phase and C phase reference current (i_b^* and i_c^*) can be calculated according to designed current shape function (12). Then, based on the motor model (1) and (2), the following voltage equation can be gained by using the Euler discretization method:

$$u_{bc}^{k+1} = \left(R - \frac{L}{T_{sc}}\right) i_{bc}^{k+1} + \frac{L}{T_{sc}} i_{bc}^{k+2} - e_{bc}^{k+1}. \tag{19}$$

In digital control system, the control period is very short, thus it can be considered that the rotor angular speed ω_m and rotor electrical angle θ are constant in the adjacent control period, which means that $e_{bc}^{k+1} \approx e_{bc}^{k}$.

Additionally, according to the deadbeat control theory, it is believed that the current value will reach its reference value at the next instant when desired voltage vector is applied. Therefore, the reference voltage vector (desired voltage vector) is the key variable to achieve the current deadbeat control. In this article, this reference voltage vector can be obtained based on (19), when i_b^{k+2} and i_c^{k+2} in (19) are equal to the reference value i_b^* and i_c^*. Then, the reference voltage (u_{bc}^*) that is needed to realize the deadbeat current control can be expressed as (20). Next, SVPWM modulation strategy is used to control the inverter to output the target voltage (u_{bc}^*). At this time, the current of the OW-PMSM system can reach the reference value at next control period, and realize the tracking of the reference currents

$$u_{bc}^* = \left(R - \frac{L}{T_{sc}}\right) i_{bc}^{k+1} + \frac{L}{T_{sc}} i_{bc}^* - e_{bc}^k \tag{20}$$

where current i_{bc}^{k+1} is the predicted current at the next control instant. Based on (1) and (2), this predicted current can be obtained by forward Euler discretization method as follows:

$$i_{bc}^{k+1} = \left(1 - R\frac{T_{sc}}{L}\right) i_{bc}^{k} + \frac{T_{sc}}{L}\left(u_{bc}^k - e_{bc}^k\right) \tag{21}$$

where T_{sc} is the switching period.

2) SVPWM Modulation: The conventional fault-tolerant topology consists of four legs and eight switching devices. Current hysteresis control is the main way to coordinate control of switching devices to achieve fault-tolerant operation. However, the proposed topology is composed of three-leg inverter which is the same as the traditional two-level inverter. Therefore, the existing SVPWM technology can be easily used to replace the hysteresis control.

It is well known that the implementation of SVPWM can be divided into three steps: sector judgment, active time calculation, and duty cycle calculation. The calculation of active time and duty cycle can be obtained by using the principle of volt-second balance and the principle of minimum switching frequency, which is the same as conventional SVPWM method and not explain in detail in this article. It should be emphasized that the sector judgment and voltage limitation are different in the proposed topological modulation.

Sector judgment: the sector where the voltage vector is located is determined by the following parameters:

$$\begin{cases} U_1 = u_\alpha \\ U_2 = u_\beta - \sqrt{3} u_\alpha \\ U_3 = -u_\beta - \sqrt{3} u_\alpha. \end{cases} \tag{22}$$

Then the sector number can be gained based on (22)

$$N_{\text{sector}} = A + 2B + 4C \tag{23}$$

where

$$A = \begin{cases} 1, U_1 > 0 \\ 0, U_1 \le 0 \end{cases}; B = \begin{cases} 1, U_2 > 0 \\ 0, U_2 \le 0 \end{cases}; C = \begin{cases} 1, U_3 > 0 \\ 0, U_3 \le 0. \end{cases}$$

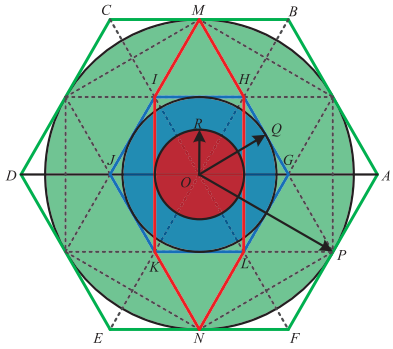

Fig. 8. Linear modulation ranges of voltage vectors under different operation conditions.

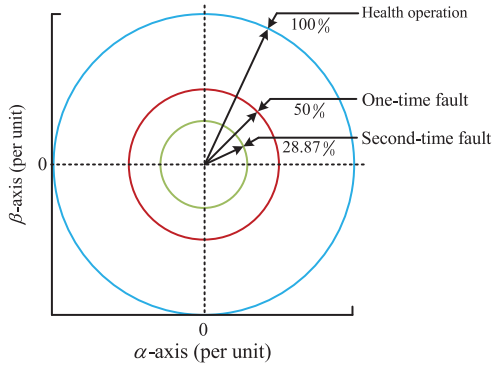

Fig. 9. Voltage vector limit in different operation condition.

Voltage limitation: for the proposed fault-tolerant topology, the linear modulation range of SVPWM is shown as circle OR in the Fig. 8. To ensure that the sum of working time of the two candidate voltage vectors in the control process does not exceed the switching period, the following constrains should be applied to t_1 and t_2 (t_1 is the active time for the first voltage vector and t_2 is for the second one)

$$t_{1\,\mathrm{or}\,2} = \begin{cases} t_{1\,\mathrm{or}\,2}, & t_1 + t_2 \le T \\ \frac{t_{1\,\mathrm{or}\,2}}{t_1+t_2} T, & t_1 + t_2 > T \end{cases} \tag{24}$$

where

$$T = \begin{cases} T_{\mathrm{sc}}, & N_{\mathrm{sector}} = 1, 6 \\ \frac{T_{\mathrm{sc}}}{\sqrt{3}}, & N_{\mathrm{sector}} = 2, 3, 4, 5. \end{cases}$$

IV. Output Capability Analysis of the Proposed Fault-Tolerant System

Due to the lack of the bridge leg and the sharing of the bridge leg, the output capability of fault-tolerant system is inevitably affected. In this section, the output performance of the proposed fault-tolerant system will be analyzed quantitatively.

A. Voltage and Current Limits of Inverter

1) Utilization Ratio of DC Voltage: Linear modulation ranges of voltage vector formed by normal topology and two kinds of fault-tolerant topologies (one-time and second-time fault-tolerant topology) are shown in Fig. 8, and the definition of voltage utilization is shown in the following equation:

$$m = \frac{U_{l1m}}{U_{\mathrm{dc}}}. \tag{25}$$

In (25), U_{l1m} is the amplitude of the output fundamental line voltage and U_{dc} is the dc voltage.

Under the normal operating condition, the OW-PMSM is powered by dual healthy inverter. In this topology, voltage vectors of hexagonal A, B, C, D, E, F and their inner regions can be synthesized, and the maximum linear modulation region is the hexagonal tangential circle OP. Hence, the radius OP of the tangential circle is the maximum amplitude of the phase voltage that can be output by linear modulation, which is $2U_{\mathrm{dc}}/\sqrt{3}$. According to the relationship between line voltage and phase voltage and (25), it is not difficult to conclude that the maximum utilization ratio of dc voltage under linear modulation is 2.

However, in the one-time fault-tolerant topology, voltage vectors of hexagonal G, H, I, J, K, L, and their inner regions can be synthesized by using voltage vector u_1–u_6. And the radius OQ of the tangential circle is the maximum amplitude of the phase voltage that can be output by linear modulation, which is $U_{\mathrm{dc}}/\sqrt{3}$. In this case, the utilization ratio of dc voltage is 1.

Similarly, in the proposed second-time fault-tolerant topology, u_2, u_7, u_3, u_5, u_8, and u_6 is the basic vectors for synthesizing the target voltage vector. And the range of voltage vectors that can be synthesized is a hexagon formed by H, M, I, K, N, and L and its internal region. The linear modulation region is the hexagonal tangential circle OR. OR $= U_{\mathrm{dc}}/3$ is the maximum output phase voltage under linear modulation in the proposed fault-tolerant topology, so the maximum utilization ratio of dc voltage is $1/\sqrt{3}$.

The results show that the dc voltage utilization ratio of the one-time fault-tolerant topology is 50% lower than that of the normal operation topology, while the proposed second-time fault-tolerant topology is 42.3% lower than that of one-time fault-tolerant topology. And the voltage limits of inverter under different operation modes are shown in Fig. 9.

2) Current Limit of Inverter: Because the second-time fault-tolerant topology adopts the structure of shared bridge leg, the shared leg will inevitably affect the current limit of the inverter. Next, the current flowing through the shared leg will be quantitatively analyzed.

It can be seen from the relevant derivation in this article that the current of healthy phase satisfies (12) under the proposed second-time fault-tolerant control strategy. According to Fig. 3 and Kirchhoff's current law, it can be known that the current of power semiconductors on the shared leg satisfy

$$i_{\mathrm{share}} = i_b - i_c = -I_m \left[\sin(\theta - 5\pi/6) - \sin(\theta + 5\pi/6)\right]. \tag{26}$$

Further simplification obtains

$$i_{\mathrm{share}} = I_m \cos\theta. \tag{27}$$

According to (12) and (27), it can be found that the amplitude of current flowing through all inverter power semiconductors is I_m, which is the same as that of the healthy operation of the

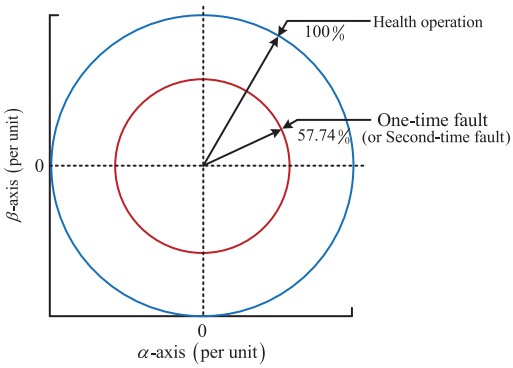

Fig. 10. Current vector limit in different operation condition.

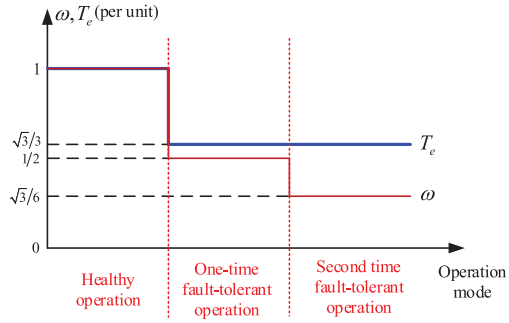

Fig. 11. Comparison of torque and speed output capacity under different operation mode.

OW-PMSM system, so the current capacity of the shared leg is also the same as that of the health system. However, since the OW-PMSM system changes from three-phase operation to two-phase operation after fault occurs, the current vector will be reduced to 57.74% of the healthy operation after the fault occurs according to the principle of coordinate transformation, which is as shown in Fig. 10.

B. Output Capability Analysis

The output capability performance of the OW-PMSM system under different operation conditions can be analyzed according to the relation expression of power, speed and torque, which is shown as follows:

$$P_m = \omega_m T_e. \tag{28}$$

1) In Normal Condition: Under the healthy condition, the three-phase voltage can be expressed as follows:

$$\begin{cases} u_a = -U_m \sin(\theta) \\ u_b = -U_m \sin(\theta - 2\pi/3) \\ u_c = -U_m \sin(\theta + 2\pi/3) \end{cases} \tag{29}$$

where U_m is the amplitude of the three-phase voltage. Then, the power of the three-phase system can be expressed as follows:

$$P_{eN} = u_a i_a + u_b i_b + u_c i_c. \tag{30}$$

Combining the three-phase voltage [in (29)] and current [in (4)] the power expression of normal condition can be obtained as follows:

$$P_{eN\text{healthy}} = \frac{3}{2} U_m I_m. \tag{31}$$

2) In Fault-Tolerant Condition: Taking A-phase open-circuit as example, the current and voltage of phase A are both 0. Under this condition, according to the derivation of fault-tolerant control in Section III, it can be known that the current of healthy phase windings is (12). As for the voltage, constrained by the electrical structure, since the space position of windings does not change before and after the fault, its electrical characteristics will not change, so the voltage of phase B and phase C meets the following:

$$\begin{cases} u_b = -U'_m \sin(\theta - 2\pi/3) \\ u_c = -U'_m \sin(\theta + 2\pi/3). \end{cases} \tag{32}$$

Then, the power expression of the fault-tolerant system can be obtained as follows:

$$P_{eN\text{fault}} = \frac{\sqrt{3}}{2} U'_m I_m. \tag{33}$$

Based on the above analysis of the voltage utilization ratio, the relationship between the normal condition power $(P_{eN\text{healthy}})$ and the fault condition powers (one-time fault power $P_{eN-4leg}$ and two-time fault power $P_{eN-3leg}$) can be gained as follows:

$$\begin{cases} P_{eN\_4leg} = \frac{\sqrt{3}}{6} P_{eN\text{healthy}} \\ P_{eN\_3leg} = \frac{1}{6} P_{eN\text{healthy}}. \end{cases} \tag{34}$$

Therefore, under the fault condition, the relationship during rated power, rated speed, and rated torque can be obtained as follows:

$$\begin{cases} P_{eN\_4leg} = \frac{\sqrt{3}}{6} P_{eN\text{healthy}} = \frac{\sqrt{3}}{6} \omega_{mN} T_{eN\text{healthy}} \\ P_{eN\_3leg} = \frac{1}{6} P_{eN\text{healthy}} = \frac{1}{6} \omega_{mN} T_{eN\text{healthy}} \end{cases} \tag{35}$$

where ω_{mN} and $T_{eN\text{healthy}}$ are rated speed and rated torque of the normal condition, respectively.

In addition, according to (5) and (18), the rated torque relation between the normal condition and the fault condition (including one-time fault and second-time fault) can be expressed as follows:

$$T_{eN\text{fault}} = \frac{\sqrt{3}}{3} T_{eN\text{healthy}}. \tag{36}$$

Then, according to (35) and (36), the rated speed relation between the normal condition and the fault-tolerant condition can be obtained as follows:

$$\begin{cases} \omega_{mN\_4\text{leg}} = \frac{P_{mN\_4\text{leg}}}{T_{eN\text{fault}}} = \frac{1}{2} \omega_{mN} \\ \omega_{mN\_3\text{leg}} = \frac{P_{mN\_3\text{leg}}}{T_{eN\text{fault}}} = \frac{\sqrt{3}}{6} \omega_{mN}. \end{cases} \tag{37}$$

According to the theoretical analysis above, the output capacity of the OW-PMSM system under different operation modes (shown in Fig. 11) can be obtained. And the following conclusion can be drawn: compared with the health condition, the one-time fault-tolerant topology and control strategy will sacrifice 42.26%

TABLE III
PARAMETERS OF OW-PMSM

DC-bus voltage	320 V
Rated power	1.25 kW
Rated speed	2000 rpm
Rated torque	6 N.m
Number of pole pairs	2
Stator phase resistance	1.5 Ω
d- and q-axis inductances	6.6 mH
Flux linkage of permanent magnets	0.4 Wb
Third harmonic component of permanent magnetic flux linkage	0.0059152 Wb

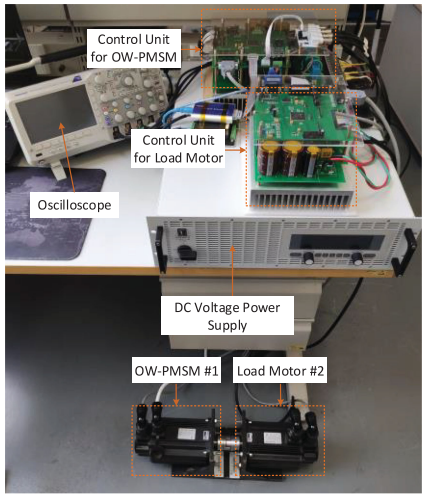

Fig. 12. Experimental platform of system.

torque capacity and 50% speed capacity when the system runs at the rated operating point; on the other hand, the second-time fault-tolerant topology will sacrifice 42.26% speed capacity and maintain the same torque output ability when it runs at rated operating point under the proposed control strategy, compared with the one-time fault-tolerant topology.

V. EXPERIMENTAL RESULTS

To verify the feasibility of the proposed fault-tolerant topology and the control performance of the proposed control strategy, experimental results are provided in this section. The fault-tolerant four-leg topology (one-time fault-tolerant topology) and its control method reported by [25] are used to compare with the proposed topology (second-time fault-tolerant topology) and control strategy. The relevant parameters of the OW-PMSM used in the experiment are shown in Table III.

A. Introduction of Experimental Platform

The hardware platform based on TI digital processor TMS320F28335 is built for the experiment of this article, as shown in Fig. 12. Two standard three-phase two-level inverters of the dual inverter adopt the IPM with the model of PS21869-AP, the TRIAC model in the fault-tolerant topology is BAT16-100B, and the dc bus of the platform is powered by the dc voltage power supply (EA-PS 9500_30) with the value of 320 V. Control unit for OW-PMSM is used to verify the control strategy, while control unit for load motor is used for loading, and the position sensors of the two motors are 2500-line incremental photoelectric encoders with a solution of 10 000. During the operation of the OW-PMSM system, the control frequency is set to 15 kHz.

During the experiments, four kinds of information are needed to be observed: current, speed, torque, and flux. The measured phase current is directly measured by Tektronix A622 ac/dc current probe, and the rest information is obtained by the DA output of the controller (TMS320F28335). Using the position sensor and current transformer (LA 100-p) contained in the platform to detect the relevant information, and then using the controller to process the data, respectively, the information of speed and I_q can be obtained; the back EMFs, torque, and flux information during the operation of the drive system are calculated by the controller based on the mathematical model, wherein the mathematical models of back EMFs and torque are (2) and (3), respectively, and the mathematical model of flux is as shown in the following equation:

$$\begin{cases} \psi_d = L_d I_d + \psi_f \\ \psi_q = L_q I_q \\ \phi = \sqrt{\psi_d^2 + \psi_q^2} \end{cases} \tag{38}$$

where L_d and L_q are the components of stator inductance on d-axis and q-axis, respectively, for the surface-mounted OW-PMSM used in the experiment $L_d = L_q = L$ is satisfied; ψ_d is the component of the flux in the d-axis, ψ_q is the component of the flux in the q-axis, and ϕ is the amplitude of flux shown in the experimental results. Current I_d and I_q can be obtained by the following equation:

$$\begin{bmatrix} I_d \\ I_q \end{bmatrix} = \frac{2}{3} \begin{bmatrix} \cos\theta \cos(\theta - 2\pi/3) \cos(\theta + 2\pi/3) \\ \sin\theta \sin(\theta - 2\pi/3) \sin(\theta + 2\pi/3) \end{bmatrix} \begin{bmatrix} i_a \\ i_b \\ i_c \end{bmatrix}. \tag{39}$$

B. Steady-State Performance Evaluation

Firstly, in order to verify the effect of the torque optimization method on the proposed fault-tolerant OW-PMSM system, the following experiment is carried out: The motor speed is given to 500 r/min with load torque of 3.46 N·m. The experimental results are shown in Fig. 13.

It can be found that the waveform difference of the fault-tolerant system before harmonic injection and after harmonic injection exists. Compared with the system performance without harmonic injection, the output torque under the control of torque optimization strategy has smaller fluctuations. In detail, torque fluctuation is 0.8 N·m before harmonic injection, and torque fluctuation is reduced to 0.45 N·m after harmonic is injected. For the flux ripple, harmonic injection will have a negative impact on it, and its value increases from 0.003 to 0.0035 Wb. In addition, since the proposed torque optimization control strategy is realized by injecting harmonic into the amplitudes of B-phase current and C-phase current, the strategy will inevitably have negative impacts on the current, which can be confirmed from

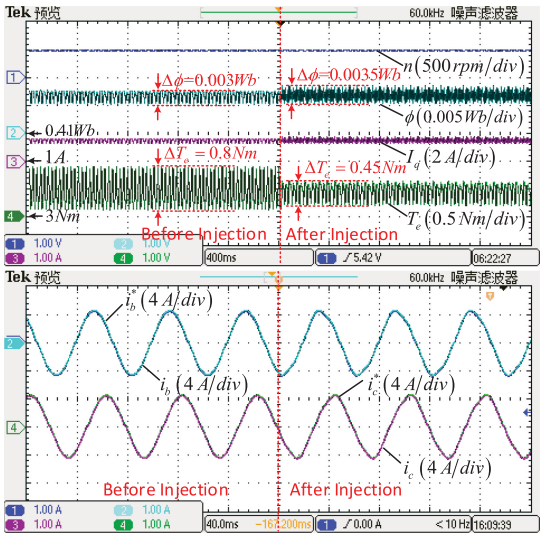

Fig. 13. Effect of torque optimization strategy of the proposed topology.

TABLE IV
PERFORMANCE COMPARISON TABLE

	Current THD	Torque ripple	Flux ripple
Healthy topology	5.24%	0.15 Nm	0.001 Wb
One-time topology	4.36%	0.92 Nm	0.003 Wb
Second time topology	5.96%	0.48 Nm	0.0035 Wb

(It needs to be explained that for the same load torque, because the phase current required by the healthy system is smaller, the current THD will get higher).

the results of current waveforms. After harmonic injection, the THD value of current will increase from 4.33% to 5.96%. It can also be seen from the experimental results that the current waveforms have a slight distortion after harmonic injection.

Next, the steady-state performance comparison between healthy topology, one-time fault-tolerant topology, and the proposed fault-tolerant topology (second-time fault-tolerant topology) is evaluated through experiments. According to (34), (35), and the parameters of the OW-PMSM shown in Table III, it can be noticed that the rated speed and rated torque of the proposed fault-tolerant topology is 577.4 r/min and 3.46 N·m, respectively. Therefore, in order to test the control performance of the proposed fault-tolerant topology (and the proposed control method) under the rated operation state, the given speed reference and load torque are set to 577.4 r/min and 3.46 N·m, respectively. The experimental results are shown in Fig. 14 and Table IV.

From the experimental results, it can be concluded that the torque ripple and flux ripple of the OW-PMSM will increase whether it is the one-time fault or the second-time fault, but the torque optimization strategy proposed in this article significantly suppresses the torque fluctuation (although the current THD and flux ripple are increased due to the addition of the harmonic current). The proposed second-time fault-tolerant system can operate smoothly at its rated operating point, and has better

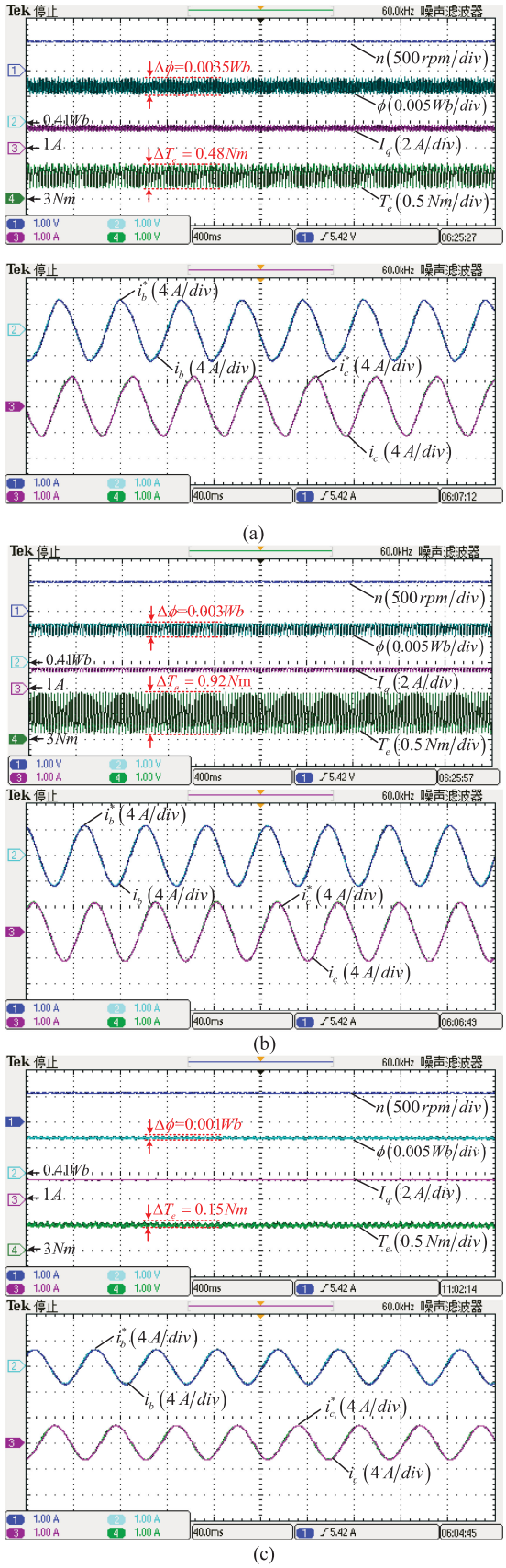

Fig. 14. Steady-state experimental results. (a) Proposed second-time topology. (b) One-time topology. (c) Healthy topology.

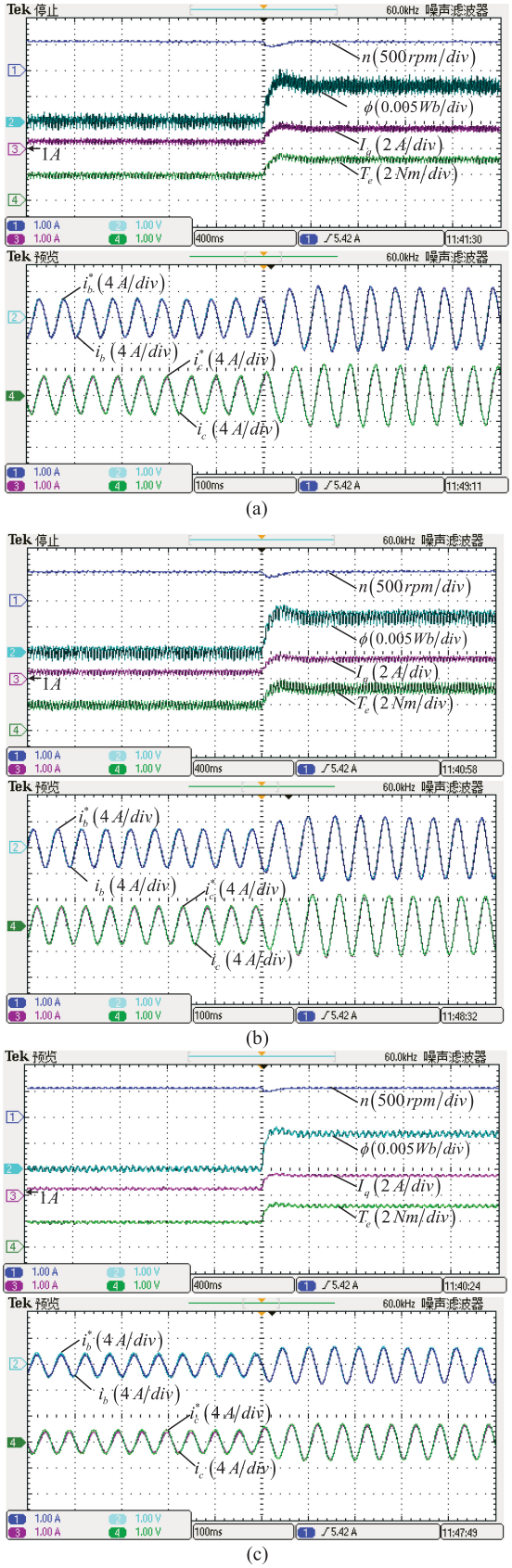

Fig. 15. Dynamic experimental results when the load torque suddenly changes from 1.98 to 3.46 N·m. (a) Proposed second-time topology with the proposed control strategy. (b) One-time topology with its control strategy. (c) Healthy topology with its control strategy.

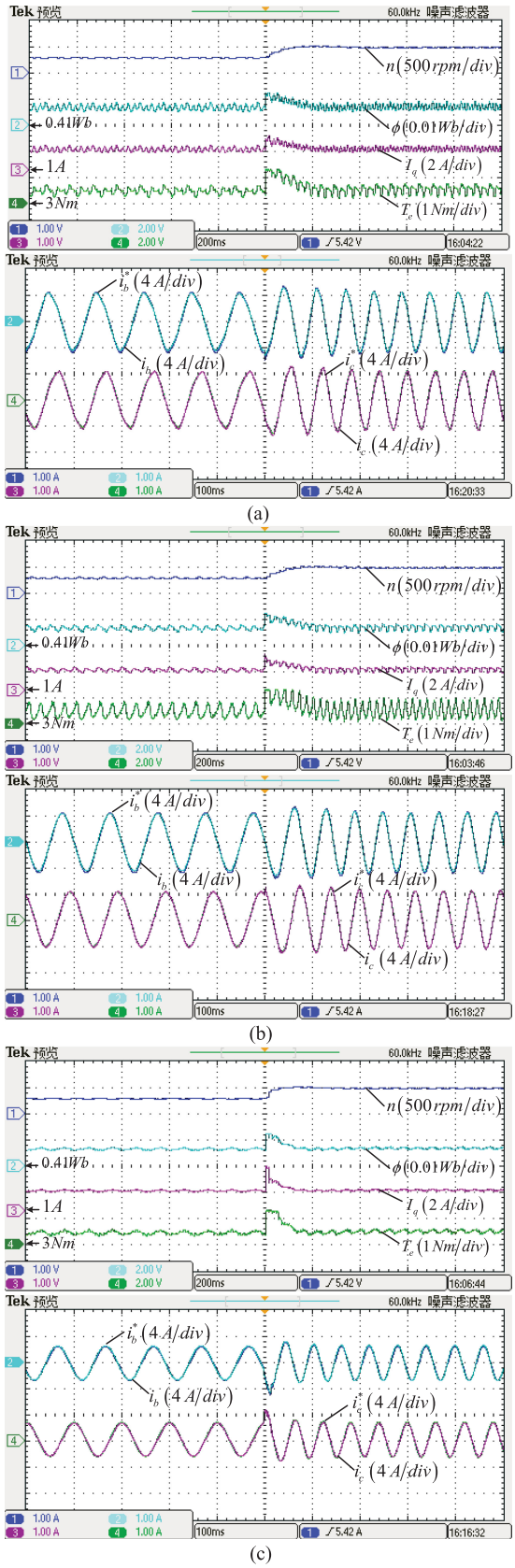

Fig. 16. Dynamic experimental results when the speed suddenly changes from 300 to 500 r/min. (a) Proposed second-time topology with the proposed control strategy. (b) One-time topology with its control strategy. (c) Healthy topology with its control strategy.

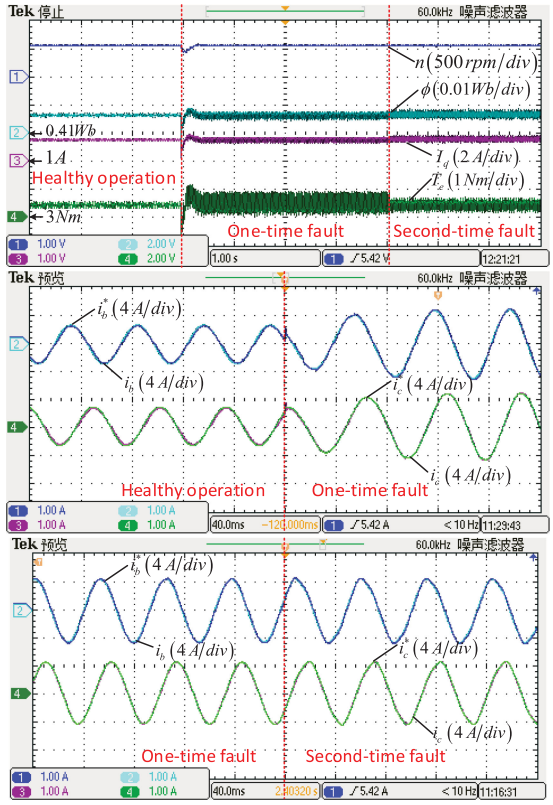

Fig. 17. Experimental results of operation mode switching.

steady-state output performance under the proposed control strategy, compared with the one-time fault-tolerant system.

C. Dynamic Performance Evaluation

In order to evaluate the performance of the proposed fault-tolerant topology and its control strategy in dynamic response, the OW-PMSM system dynamic test is carried out. First, the load test is carried out, and the experimental condition is set to a rated speed of 577.4 r/min with the load torque suddenly change from 1.98 N·m to rated torque 3.46 N·m. The comparative experiment results between healthy topology, one-time and proposed second-time fault-tolerant system are shown in Fig. 15, it can be seen that both systems have good dynamic response. When the load torque suddenly changes, the speed of the two systems can quickly recover to steady state. The proposed second-time fault-tolerant system has dynamic performance comparable to the one-time fault-tolerant system.

Next, the speed transient test is carried out to further verify the dynamic performance of the proposed fault-tolerant topology and its control strategy. The experimental condition is set to a rated load torque of 3.46 N·m with the speed suddenly changing from 300 to 500 r/min. The experiment results are shown in Fig. 16, from the experiment results, it can be found that the OW-PMSM system can follow the change of the speed command well, and reach a new steady state in a short time. Combined with the two kinds of dynamic test, it can be concluded that the proposed fault-tolerant topology and control strategy have a good dynamic performance.

D. Operation Mode Switching Test

In order to verify the feasibility of the proposed fault-tolerant topology, switching test from the healthy mode to one-time topology and then to second-time topology is carried out. In the experiment, the speed is set to 577.4 r/min with a load torque of 3.46 N·m. Assuming that the one-time fault is A-phase open-circuit, and the second-time fault occurs between B and C' bridge legs, the switching process of the OW-PMSM system is shown in Fig. 17. The experimental results certificate the feasibility of the proposed topology and the proposed control strategy.

VI. Conclusion

A kind of second-time fault-tolerant topology and control method is proposed in this article, in order to further improve the continuous operation ability of the OW-PMSM system under fault condition. The proposed fault-tolerant topology and the proposed control method can realize the smooth operation of the second-time open-circuit fault of remaining inverter bridge arm under the condition of one-phase open-circuit fault operation. In addition, a torque optimization strategy is presented. This strategy based on torque equation can realize the suppression of system torque ripple by injecting harmonic into current amplitude to make the system run with more security and stability.

References

[1] X. Zhang, B. S. Hou, and Y. Mei, "Deadbeat predictive current control of permanent-magnet synchronous motors with stator current and disturbance observer," *IEEE Trans. Power Electron.*, vol. 32, no. 5, pp. 3818–3834, May 2017.

[2] Z. Xiaoguang, Z. Liang, and Z. Yongchang, "Model predictive current control for PMSM drives with parameter robustness improvement," *IEEE Trans. Power Electron.*, vol. 34, no. 2, pp. 1645–1657, Feb. 2019.

[3] X. Zhang and B. S. Hou, "Double vectors model predictive torque control without weighting factor based on voltage tracking error," *IEEE Trans. Power Electron.*, vol. 33, no. 3, pp. 2368–2380, Mar. 2018.

[4] S. Wei, S. Huang, J. Gao, and Q. Zhang, "Research on the internal short circuit fault tolerant operation of the PMSM," in *Proc. IEEE Conf. Expo. Transp. Electrific. Asia-Pac.*, 2014, pp. 1–4.

[5] N. Sujitha, B. Karthika, R. H. Kumar, and M. Sasikumar, "Analysis of hybrid PWM control schemes for cascaded multilevel inverter fed industrial drives," in *Proc. Int. Conf. Circuits, Power Comput. Technol.*, 2014, pp. 745–750.

[6] P. Sandulescu, F. Meinguet, X. Kestelyn, E. Semail, and A. Bruyère, "Control strategies for open-end winding drives operating in the flux-weakening region," *IEEE Trans. Power Electron.*, vol. 29, no. 9, pp. 4829–4842, Sep. 2014.

[7] A. M. S. Mendes and A. J. Marques Cardoso, "Fault-tolerant operating strategies applied to three-phase induction-motor drives," *IEEE Trans. Ind. Electron.*, vol. 53, no. 6, pp. 1807–1817, Dec. 2006.

[8] R. K. Gupta, K. K. Mohapatra, A. Somani, and N. Mohan, "Direct-matrix-converter-based drive for a three-phase open-end-winding AC machine with advanced features," *IEEE Trans. Ind. Electron.*, vol. 57, no. 12, pp. 4032–4042, Dec. 2010.

[9] Y. Lee and J. Ha, "Hybrid modulation of dual inverter for open-end permanent magnet synchronous motor," *IEEE Trans. Power Electron.*, vol. 30, no. 6, pp. 3286–3299, Jun. 2015.

[10] K. A. Corzine, S. D. Sudhoff, and C. A. Whitcomb, "Performance characteristics of a cascaded two-level converter," *IEEE Trans. Energy Convers.*, vol. 14, no. 3, pp. 433–439, Sep. 1999.

[11] Q. An, J. Liu, Z. Peng, L. Sun, and L. Sun, "Dual-space vector control of open-end winding permanent magnet synchronous motor drive fed by dual inverter," *IEEE Trans. Power Electron.*, vol. 31, no. 12, pp. 8329–8342, Dec. 2016.

[12] H. Nian, Y. Zhou, and H. Zeng, "Zero-sequence current suppression strategy for open winding PMSG fed by semicontrolled converter," *IEEE Trans. Power Electron.*, vol. 31, no. 1, pp. 711–720, Jan. 2016.
[13] W. Zhou, D. Sun, M. Chen, and B. Lin, "Simplified PWM for fault tolerant control of open winding PMSM fed by hybrid inverter," in *Proc. IEEE Energy Convers. Congr. Expo.*, 2015, pp. 2912–2918.
[14] J. A. Restrepo, A. Berzoy, A. E. Ginart, J. M. Aller, R. G. Harley, and T. G. Habetler, "Switching strategies for fault tolerant operation of single DC-link dual converters," *IEEE Trans. Power Electron.*, vol. 27, no. 2, pp. 509–518, Feb. 2012.
[15] C. Ruan, W. Hu, H. Nian, and D. Sun, "Open-phase fault control in open-winding PMSM system with common DC bus," in *Proc. IEEE Appl. Power Electron. Conf. Expo.*, 2019, pp. 1052–1056.
[16] N. K. Nguyen, F. Meinguet, E. Semail, and X. Kestelyn, "Fault-tolerant operation of an open-end winding five-phase PMSM drive with short-circuit inverter fault," *IEEE Trans. Ind. Electron.*, vol. 63, no. 1, pp. 595–605, Jan. 2016.
[17] W. Zhao, P. Zhao, D. Xu, Z. Chen, and J. Zhu, "Hybrid modulation fault-tolerant control of open-end windings linear vernier permanent-magnet motor with floating capacitor inverter," *IEEE Trans. Power Electron.*, vol. 34, no. 3, pp. 2563–2572, Mar. 2019.
[18] Y. Wang, T. A. Lipo, and D. Pan, "Robust operation of double-output AC machine drive," in *Proc. Int. Conf. Power Electron. ECCE Asia*, 2011, pp. 140–144.
[19] N. M. A. Freire and A. J. M. Cardoso, "A fault-tolerant direct controlled PMSG drive for wind energy conversion systems," *IEEE Trans. Ind. Electron.*, vol. 61, no. 2, pp. 821–834, Feb. 2014.
[20] N. M. A. Freire and A. J. Marques Cardoso, "Fault-tolerant converter for AC drives using vector-based hysteresis current control," in *Proc. 9th IEEE Int. Symp. Diagnostics Electric Mach., Power Electron. Drives*, 2013, pp. 249–256.
[21] M. Shahbazi, P. Poure, S. Saadate, and M. R. Zolghadri, "FPGA-based reconfigurable control for fault-tolerant back-to-back converter without redundancy," *IEEE Trans. Ind. Electron.*, vol. 60, no. 8, pp. 3360–3371, Aug. 2013.
[22] I. Jlassi and A. J. M. Cardoso, "Fault-tolerant back-to-back converter for direct-drive PMSG wind turbines using direct torque and power control techniques," *IEEE Trans. Power Electron.*, vol. 34, no. 11, pp. 11215–11227, Nov. 2019.
[23] D. Zhou, J. Zhao, and Y. Li, "Model-predictive control scheme of five-leg AC–DC–AC converter-fed induction motor drive," *IEEE Trans. Ind. Electron*, vol. 63, no. 7, pp. 4517–4526, Jul. 2016.
[24] S. Yang, X. Sun, M. Ma, X. Zhang, and L. Chang, "Fault detection and identification scheme for dual-inverter fed OEWIM drive," *IEEE Trans. Ind. Electron.*, vol. 67, no. 7, pp. 6112–6123, Jul. 2020.
[25] Q. An, M. H. Duan, L. Sun, and G. L. Wang, "SVPWM strategy of post-fault reconfigured dual inverter in open-end winding motor drive systems," *Electron. Lett.*, vol. 50, no. 17, pp. 1238–1240, Aug. 2014.

Xiaoguang Zhang (Member, IEEE) received the B.S. degree from the Heilongjiang Institute of Technology, Harbin, China, in 2007, and the M.S. and Ph.D. degrees from the Harbin Institute of Technology, Harbin, China, in 2009 and 2014, respectively, all in electrical engineering.

He is currently a Distinguished Professor with the North China University of Technology, Beijing, China. From 2012 to 2013, he was a Research Associate with Wisconsin Electric Machines and Power Electronics Consortium, University of Wisconsin–Madison, Madison. He has published more than 40 technical papers in the area of motor drives. His current research interests include power electronics and electric machines drives.

Chi Xu received the B.S. degree in electrical engineering in 2018 from the North China University of Technology, Beijing, China, where he is currently working toward the M.S. degree.

His current research interests include motor drives.